Front. Chem. Sci. Eng. 2025, 19(6): 52
https://doi.org/10.1007/s11705-025-2553-2

RESEARCH ARTICLE

Innovative deep learning method for predicting the state of health of lithium-ion batteries based on electrochemical impedance spectroscopy and attention mechanisms

Cheng Lou[1,3*], Jianhao Zhang[2*], Xianmin Mu[2], Fanpeng Zeng[4], Kai Wang (✉)[1]

1 School of Electrical Engineering, Qingdao University, Qingdao 266000, China
2 School of Electrical Engineering, Dalian University of Technology, Dalian 116081, China
3 Zaozhuang Power Supply Company, Shandong Electric Power Company, State Grid Corporation of China, Zaozhuang 277000, China
4 Jiangsu Linyang Energy Storage Technology Co., Ltd., Nanjing 210019, China

Abstract Electrochemical impedance spectroscopy plays a crucial role in monitoring the state of health of lithium-ion batteries. However, effective feature extraction often relies on limited information and prior knowledge. To address this issue, this paper presents an innovative approach that utilizes the gramian angular field method to transform raw electrochemical impedance spectroscopy data into image data that is easily recognizable by convolutional neural networks. Subsequently, the convolutional block attention module is integrated with bidirectional gated recurrent unit for state of health prediction. First, convolutional block attention module is applied to the electrochemical impedance spectroscopy image data to enhance key features while suppressing redundant information, thereby effectively extracting representative battery state features. Subsequently, the extracted features are fed into a bidirectional gated recurrent unit network for time series modeling to capture the dynamic changes in battery state of health. Experimental results show a significant improvement in the accuracy of state of health predictions, highlighting the effectiveness of convolutional block attention module in feature extraction and the advantages of bidirectional gated recurrent unit in time series forecasting. This research provides an attention mechanism-based feature extraction solution for lithium-ion battery health management, demonstrating the extensive application potential of deep learning in battery state monitoring.

Keywords electrochemical impedance spectroscopy, state of health, gramian angular field, convolutional block attention module, bidirectional gated recurrent units

Received March 4, 2025; accepted March 24, 2025; online April 20, 2025

E-mail: wangkai@qdu.edu.cn

*These authors contributed equally to the work.

1 Introduction

With the rapid proliferation of electric vehicles and renewable energy, the demand for battery lifespan prediction is continuously growing [1−5]. Lithium-ion batteries, in particular, have a widespread application in various fields, including electric vehicles and energy storage systems, making their lifespan prediction especially critical [6−9]. Battery sensing and health status monitoring are becoming increasingly important in various areas [10−12]. Therefore, accurate lifespan prediction not only helps to identify declines in battery performance in a timely manner, but also effectively reduces the risks of failures and accidents, thereby significantly enhancing safety during use [13,14].

In battery management, the state of health (SOH) of a battery is an essential metric for assessing its performance and lifespan [15,16]. Changes in SOH directly impact the performance and safety of the battery, making its monitoring particularly important in the management of rechargeable batteries like lithium-ion batteries [17]. SOH is typically expressed as a percentage, measuring the relationship between the current health status of the battery and its optimal or initial state [18]. The calculation and estimation of SOH can be accomplished through various parameters, including internal resistance, capacity, and charge/discharge efficiency, which provide crucial quantitative evidence for evaluating battery performance [19].

As lithium-ion battery technology continues to advance, researchers have widely adopted electrochemical impedance spectroscopy (EIS) techniques, particularly in the assessment of battery performance and lifespan prediction [20]. EIS not only provides intuitive

information about the complex dynamic processes within the battery but also helps deepen the understanding of battery failure mechanisms. Additionally, as a non-destructive testing method, EIS can monitor the battery's state in real-time during charging and discharging processes, thereby supporting continuous health state assessments [21].

Currently, prediction methods for EIS can be broadly categorized into three types: experimental methods, model-based methods, and data-driven methods [22]. Experimental methods acquire battery impedance data directly through EIS testing and analyze it based on empirical evidence or heuristics. However, these methods are often limited to specific types of batteries or testing conditions, making it difficult to generalize results to other battery types [23]. In contrast, model-based methods establish equivalent circuit models of the battery and utilize EIS data to fit the parameters within the circuit [24]. While this approach can provide high accuracy, it requires complex modeling processes and lengthy computation times. In comparison, data-driven methods extract information from historical data using statistical and machine learning algorithms, offering new avenues for accurate predictions of battery health status [25]. These methods are capable of capturing complex nonlinear relationships and time-varying characteristics in EIS data, thereby improving the accuracy of SOH predictions. With advancements in data acquisition technology and analytical techniques, data-driven methods are expected to become important tools in future battery management. This approach typically involves two key stages: feature extraction and predictive model training.

During the feature extraction stage, methods can be categorized as manual and automatic. Manual feature extraction relies on the experience and knowledge of researchers to identify important features through the visualization and analysis of EIS data [26,27]. However, this approach tends to be inefficient for large data sets and is susceptible to subjective judgment, resulting in poor reproducibility and biased outcomes. In contrast, automatic feature extraction methods are more suitable for handling large-scale data sets. They can rapidly process vast amounts of EIS data, significantly enhance efficiency while reducing human errors, and improve the reproducibility of results [28]. Additionally, automatic methods may uncover implicit features or patterns that might be overlooked during manual processing by experts.

After feature extraction, model training becomes a crucial step, with methods broadly divided into machine learning and deep learning categories. Machine learning algorithms, such as Gaussian process regression (GPR) [29], support vector regression [30], random forest [31], and extreme learning machine [26], have all demonstrated good results in SOH prediction. Simultaneously, deep learning methods, including deep neural networks (DNN) [32], convolutional neural networks (CNN) [33], and recurrent neural networks (RNN) [34], show significant application potential. For example, Li et al. [35] proposed a technique that processes EIS data using CNN and combines it with a bidirectional long short-term memory (BiLSTM) model for sequence regression prediction, markedly outperforming the traditional GPR model in prediction accuracy. Additionally, Obregon et al. [32]. introduced a CAE-DNN end-to-end deep learning framework, which further improves the accuracy of battery SOH predictions and eliminates the need for manual feature extraction Meanwhile, Guo et al. [36] utilized the convolutional and pooling layers in the VGG16 neural network for unsupervised feature extraction of EIS images, automatically capturing important information related to battery SOH. In this context, Xing et al. [37] proposed an EIS SOH estimation method that combines CNN with BiLSTM and an attention mechanism. This method automatically extracts key features through CNN to prevent feature loss and enhances the extraction of important information using BiLSTM and the attention mechanism, significantly improving estimation accuracy compared to traditional methods. This study emphasizes the important role of attention mechanisms in enhancing model performance. Building on this, Zhang et al. [38] proposed a hybrid attention estimation framework that integrates electrical and EIS aging information. This framework effectively extracts and maps battery aging features through local and global attention mechanisms, combined with simulations of actual charging and discharging conditions, thus significantly improving the accuracy of lithium-ion battery SOH assessment.

Inspired by the findings of the above studies, this paper proposes an innovative method that combines the convolutional block attention module (CBAM) and bidirectional gated recurrent unit (BiGRU) for feature extraction of EIS and SOH prediction, as illustrated in Fig. 1. CBAM integrates both channel attention and spatial attention mechanisms, where the channel attention assesses the importance of different channel features and applies weighting, while the spatial attention focuses on various spatial locations within the feature maps to identify the most important features. The adaptive weighting mechanism and comprehensive feature representation capability of CBAM significantly enhance model performance on complex tasks. The extracted features are then processed by the BiGRU for SOH prediction. Compared to traditional RNN structures, BiGRU utilizes bidirectional information flow, enabling the model to simultaneously draw from both past and future states of the time series data, thereby capturing the time-varying characteristics of battery states more accurately. Moreover, the BiGRU structure has fewer parameters, offers high training efficiency, and is easy to

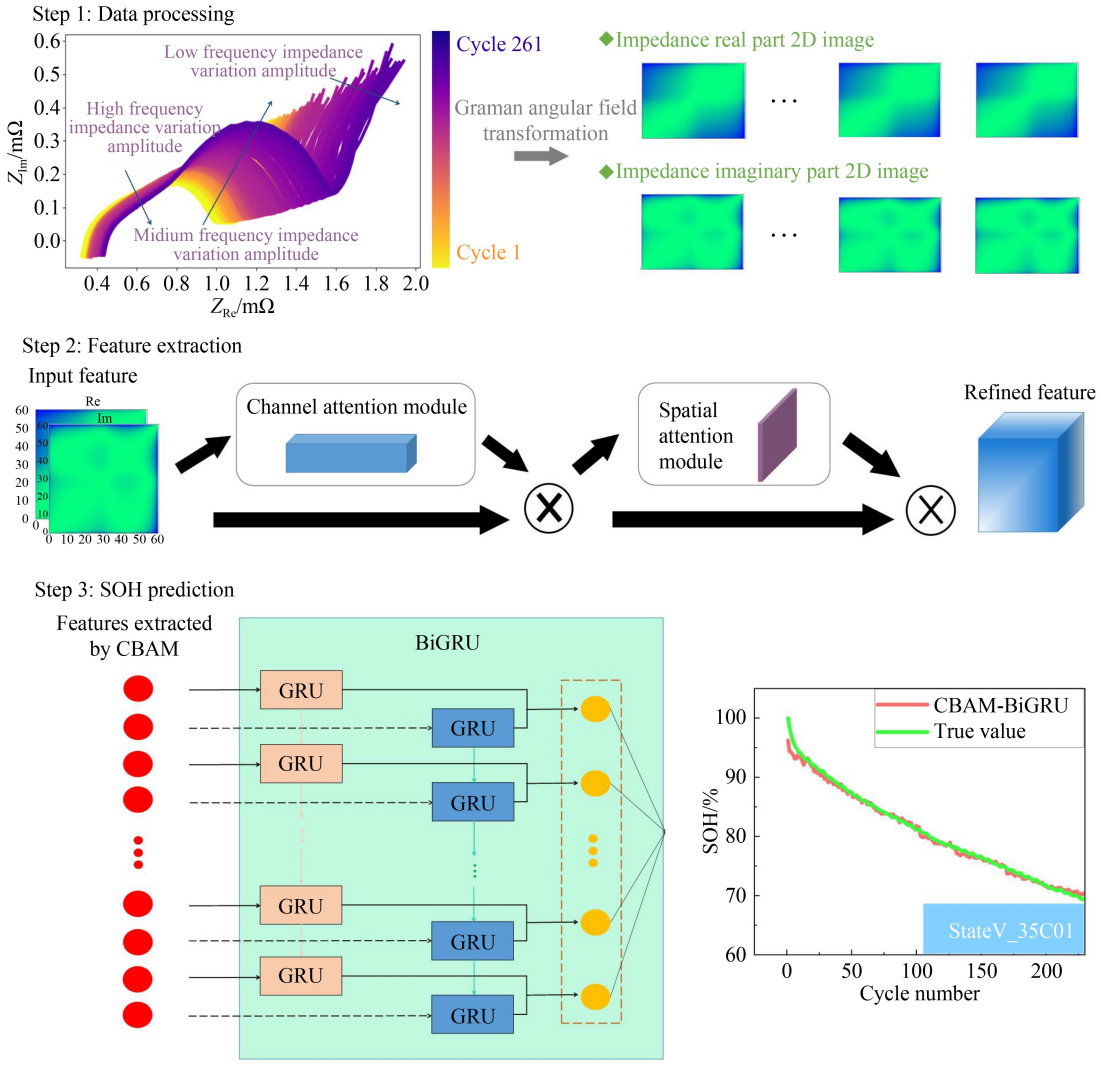

Fig. 1 SOH estimation framework for lithium batteries.

tune, which enhances the model's adaptability and real-time performance in battery SOH prediction, providing a more effective solution for the intelligent management of battery systems. The contributions of this work are mainly threefold: (1) A novel deep learning model is proposed that combines the CBAM and BiGRU, which effectively enhances the accuracy of predicting the SOH of lithium-ion batteries; (2) The CBAM technique is employed to enhance the feature extraction capability of EIS data, effectively suppressing redundant information and improving the representativeness of the features, thus laying a solid foundation for subsequent predictions; (3) Features extracted are modeled as time series using BiGRU, which accurately captures the dynamic changes in battery SOH and adapts to the varying states and performances of lithium-ion batteries during use.

The structure of the rest of this paper is organized as follows: Section 2 introduces the EIS data set used in this study; Section 3 provides a detailed explanation of the proposed SOH estimation method for lithium-ion batteries; Section 4 validates the effectiveness of the SOH estimation method; and Section 5 summarizes the contributions of this research.

2 Experimental data sources

The lithium-ion battery data set used in this study is sourced from reference [29]. The experimental subjects consist of 12 commercial Eunicell LR2032 lithium-ion coin cells, with a nominal capacity of 45 mAh and a nominal voltage of 3.6 V. The positive and negative electrode materials are $LiCoO_2$ and graphite, respectively, and the cells are separated by a composite separator made of polypropylene and polyethylene.

Initially, all batteries underwent 30 charge-discharge cycles at 25 °C. They were then placed in constant temperature environments at 25, 35, and 45 °C, where they were charged to a final voltage of 4.2 V at a constant current (CC) of 1C (45 mA), followed by discharging to 3 V at a CC of 2C. After discharging, the batteries were

allowed to rest for 15 min, during which their EIS and capacity were measured using a 5 mA excitation current. EIS data was recorded at nine different stages of the charge-discharge cycles (states I-IX in Fig. 2), but state I and state V are of interest, as this state provides a more accurate model under electrochemically stable conditions. The data set is named in the format "XXCYY," where "XX" indicates the test temperature (e.g., 25 or 45), and "YY" represents the battery number.

3 Methodology

3.1 Gramian angular field transformation

The one-dimensional data from EIS conceals many features related to the degradation of SOH. However, directly extracting these features from the one-dimensional data can be quite challenging, as it consists solely of a single sequence of values, lacking clear structural and shape information. By transforming the data into two-dimensional images, we can more intuitively observe edge and texture information within the data, thereby identifying periodicities, trends, and anomalies, which enhances the effectiveness of feature extraction.

In this study, we employ Gramian angular field (GAF) to encode the real and imaginary parts of the electrochemical impedance spectra into two-dimensional images, thereby enhancing the feature representation of EIS sequence information [39]. GAF presents the data in terms of angles, allowing it to accurately capture trends and periodic characteristics within the data. For EIS data, impedance spectra often exhibit specific trends and frequency periodicities, and GAF can effectively capture and represent these features. The following outlines the principles and formulas involved in this process.

1. Data preparation and normalization

First, the EIS curve's real and imaginary part data points are arranged into a vector:

$$X = [x_1, x_2, \ldots, x_n]. \tag{1}$$

Next, we normalize this sequence data X to the interval $[-1,1]$. The normalization formula is:

$$x_i' = \frac{2(x_i - \min(X))}{\max(X) - \min(X)} - 1, \tag{2}$$

where $\min(X)$ and $\max(X)$ are the minimum and maximum values in the data set X, respectively.

2. Polar coordinate representation

The normalized EIS sequence data can be represented in polar coordinates as follows:

Polar angle θ_i (encoded as the cosine angle):

$$\theta_i = \arccos\left(x_i'\right). \tag{3}$$

Polar radius r_i (encoded as the timestamp t_i):

$$r_i = \frac{t_i}{N}. \tag{4}$$

Here, t_i represents the timestamp for each data point, and N is the total number of data points in the EIS curve. After the transformation into polar coordinates, the representation will be:

$$(r_i, \theta_i). \tag{5}$$

The polar radius r_i and polar angle θ_i maintain all information from the normalized value x_i' and the timestamp t_i. Mathematically, this mapping is a bijective function, meaning there is a one-to-one correspondence between independent and dependent variables.

3. Inner product method in GAF

In GAF, a special inner product method is defined as:

$$\langle x_1, x_2 \rangle = \cos(\theta_1 + \theta_2). \tag{6}$$

Here, the inner product indicates the cosine of the sum of the angles of two data points after the polar transformation. This inner product reflects the similarity between the two EIS data points.

4. GAF encoding

By calculating the inner product of data points, we generate the Gramian matrix G:

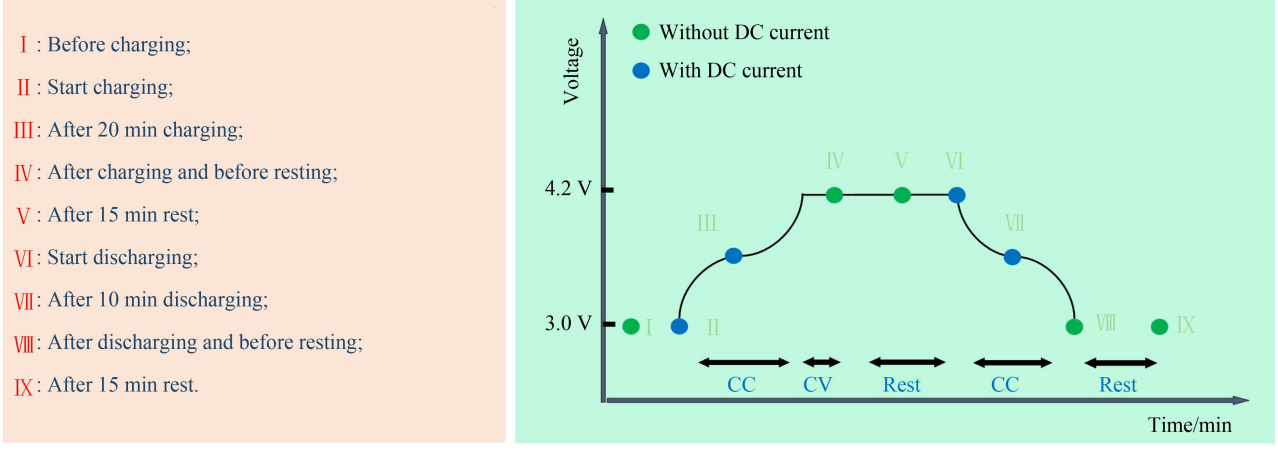

Fig. 2 Nine SOC state points of EIS data collected during CC and constant voltage (CV) charging.

$$G_{i,j} = \cos(\theta_i - \theta_j). \quad (7)$$

This step effectively encodes the one-dimensional EIS data into two dimensions, resulting in a GAF matrix with dimensions of $n \times n$, thus expanding the EIS data from one-dimensional to two-dimensional. After GAF encoding, the EIS data are mapped into two two-dimensional images representing the real and imaginary parts, as shown in Fig. 3.

The GAF method, while relatively complex in terms of computation—especially when handling large data sets—may present bottlenecks in the time and memory costs associated with calculating the GAF matrix. However, these challenges also highlight its advantages in data analysis. First, GAF transforms time series data into image format, significantly enhancing data visualization capabilities, which allows researchers to more easily recognize patterns, trends, and anomalies. Secondly, by integrating deep learning techniques such as CNN, GAF can automatically extract high-level, abstract features more efficiently and with superior performance compared to traditional manual feature extraction. Deep learning models can adaptively learn key features from the images, thereby improving classification and predictive accuracy. Additionally, the GAF method effectively captures potential nonlinear relationships in the data, which can be challenging in traditional time series analysis. By presenting electrochemical information in image format, the model can learn more complex patterns, enhancing the depth and accuracy of the analysis. For complex EIS data, the GAF transformation effectively integrates the impacts of multiple electrochemical processes, reducing the chance of information loss. This integration allows the model to consider interactions among multiple variables during analysis, leading to a more comprehensive understanding and more accurate results.

3.2 Convolutional block attention module

Feature extraction is crucial in the analysis of EIS data. Traditional methods often rely on domain knowledge and experience for manual feature selection, which is time-consuming and prone to information loss or noise interference. Moreover, the complexity of EIS data limits the reliance on human judgment due to the constraints of prior knowledge.

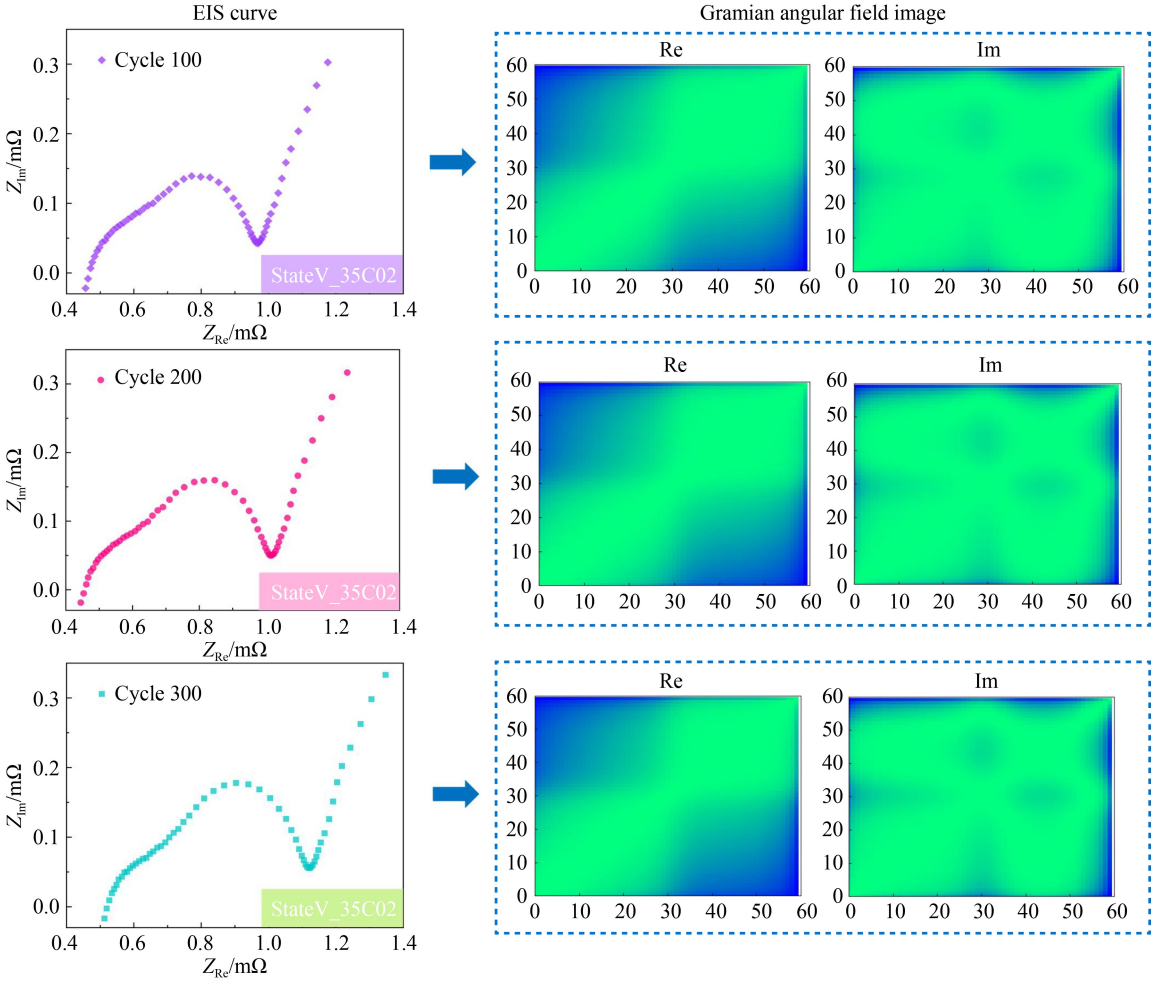

Fig. 3 EIS image processed by GAF: (a) cycle 100; (b) cycle 200; (c) cycle 300.

In this context, neural networks demonstrate strong potential due to their advantages in automatic feature extraction. Through multi-layer nonlinear transformations, neural networks can autonomously learn key features from EIS data, avoiding inherent biases in manual feature design. This optimization and adaptability based on large data sets not only improve the efficiency of feature extraction but also enhance the model's ability to capture difficult-to-identify patterns.

In this study, we employed the CBAM for feature extraction [40]. By incorporating channel attention and spatial attention mechanisms, CBAM enables the model to focus on informative channels and significant spatial regions, further enhancing the extraction capability of EIS data features. This approach effectively captures rich electrochemical information, laying a solid foundation for subsequent analysis and decision-making. Particularly in applications such as SOH assessment, monitoring of charging and discharging processes, and fault diagnosis, the capabilities of CBAM are especially important. In these scenarios, EIS data often exhibit high complexity and nonlinear characteristics, and CBAM can highlight key features closely related to battery performance, thereby enhancing the predictive accuracy and reliability of the model.

The CBAM structure consists of two main components: the channel attention module and the spatial attention module, which focus on the key channels and prominent spatial regions of the feature map, respectively. As shown in Fig. 4, the CBAM neural network architecture employed in this study utilizes the GAF to convert the real and imaginary parts of EIS data into RGB images of 60 × 60 pixels. Based on this, CBAM takes both the real and imaginary images as input and initially computes the global information of the input feature map via the channel attention module. This module generates two distinct feature descriptions through global average pooling and global max pooling, and subsequently transforms them through a fully connected layer with shared weights, using the sigmoid activation function to generate channel attention weights. These weights are then applied to the input feature map, enhancing the features of important channels while suppressing those of less important channels.

Following the completion of the channel attention module, CBAM further employs the spatial attention module to process the spatial dimensions of the feature map. This module generates spatial descriptions by performing average pooling and max pooling on the feature map after channel compression, and then calculates the spatial attention weights using convolution operations and the sigmoid activation function. This process allows the model to focus on important spatial regions within the image, thereby enhancing the spatial representation of the features. After the weighted integration of both channel and spatial attentions, CBAM outputs an enhanced feature map that emphasizes the more significant features in the EIS data, ensuring that the

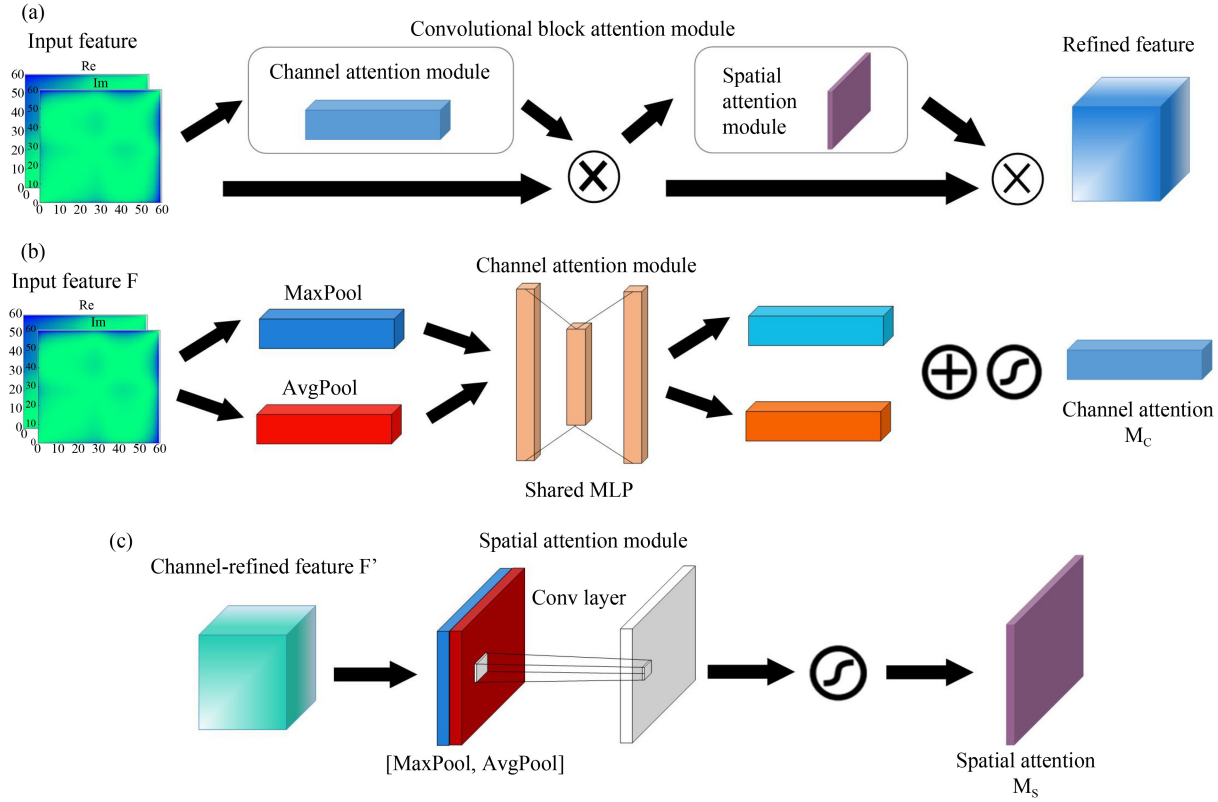

Fig. 4 CBAM overall framework: (a) convolutional block attention module; (b) channel attention module; (c) spatial attention module.

model can effectively identify key attributes related to SOH, thus providing reliable support for subsequent SOH prediction tasks.

3.3 Bidirectional gated recurrent unit

In the field of battery SOH prediction, traditional neural network methods such as feedforward neural network (FNN) [41], long short-term memory networks (LSTM) [42], and CNN all have certain limitations. Specifically, FNNs fail to effectively capture temporal features, while LSTMs may encounter overfitting issues due to their high computational complexity and storage requirements. Additionally, CNNs do not fully capture global relationships when processing time series data, which leads to inefficient utilization of contextual information.

To address these issues, this study selects gated recurrent unit (GRU) as the predictive model. GRUs have a simplified gating mechanism that can effectively capture temporal dependencies [43]. To further enhance model performance, this paper proposes the BiGRU model [44], the framework of which is illustrated in Fig. 5. BiGRU not only incorporates the advantages of GRU but also processes sequence data bidirectionally, allowing it to simultaneously capture information from both past and future, thereby enhancing the model's contextual understanding. Compared to LSTM, BiGRU effectively captures sequential information while maintaining efficient computational characteristics, particularly in complex data tasks, which significantly enhances predictive accuracy. The simplified structure of BiGRU reduces the number of parameters, thereby lowering memory consumption and computational speed, making the training and tuning process more convenient and accelerating the model development cycle. Its bidirectional structure allows for the simultaneous capture of past and future contextual information, which is crucial for real-time monitoring and analysis of EIS data, thus improving model performance more effectively. Additionally, BiGRU demonstrates better scalability in resource-constrained environments, making it suitable for deployment in embedded systems or mobile devices, thereby providing an appealing option for battery

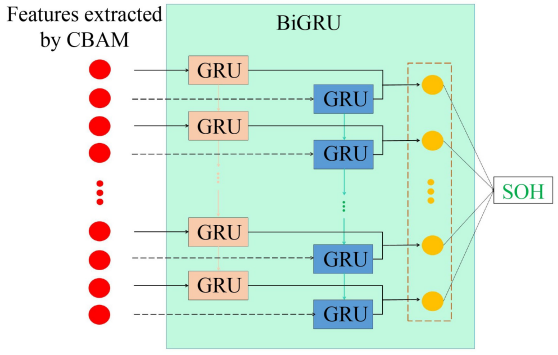

Fig. 5 The structural principles of BiGRU.

management solutions. This improvement provides BiGRU with stronger robustness and higher accuracy in battery SOH prediction, effectively addressing the shortcomings of traditional methods.

The design of BiGRU includes two GRU layers: the forward layer processes information from the beginning to the end of the sequence, while the backward layer processes information from the end to the beginning. This bidirectional mechanism enables BiGRU to effectively consider both past and future information, enhancing contextual understanding. Additionally, the built-in gating mechanisms of BiGRU, particularly the update gate and reset gate, constitute its key advantages. The update gate flexibly controls how much information from the previous state is retained in the current state to adapt to different temporal dependencies, while the reset gate adjusts the influence of the previous state when calculating the current state, thereby enhancing the ability to capture short-term dependencies. These mechanisms effectively overcome the common gradient vanishing problem faced by traditional RNNs, allowing BiGRU to excel at learning the complex relationships between long-term and short-term dependencies.

In summary, the proposed method that combines CBAM and BiGRU not only improves the accuracy of feature extraction but also enhances the expressiveness of time series models. This integrated approach offers a more precise tool for predicting battery health status and demonstrates the tremendous potential of deep learning in time series data analysis.

4 Results and discussion

To verify the effectiveness of the SOH estimation method for lithium-ion batteries proposed in this paper, we selected batteries numbered 25C01, 25C05, 35C01, and 45C01 as the test samples. During the testing process, specific batteries were used as the test set, while other batteries maintained at the same temperature were used as the training set. This design not only ensures that the model is trained and tested under similar environmental conditions but also enhances the evaluation of the model's accuracy and reliability. To further demonstrate the superiority of the proposed model, we compared the SOH estimations of three different models: CNN-GRU, CBAM-GRU, and CBAM-BiGRU. This comparison allows us to gain deeper insights into the performance differences among various models regarding SOH prediction accuracy and response speed.

4.1 Evaluation criteria

To evaluate the effectiveness of the proposed model in estimating the SOH of lithium-ion batteries, this study selects three main indicators: root mean square error

(RMSE), mean absolute error (MAE), and coefficient of determination (R^2). The comprehensive assessment of these indicators can provide a holistic reflection of the model's predictive performance. The evaluation criteria are as follows:

$$\mathrm{RMSE} = \sqrt{\frac{1}{n}\sum_{i=1}^{n}(y_i - \hat{y}_i)^2} \times 100\%, \tag{8}$$

$$\mathrm{MAE} = \frac{1}{n}\sum_{i=1}^{n}|y_i - y_i| \times 100\%, \tag{9}$$

$$\mathbf{R}^2 = 1 - \frac{\sum_{i=1}^{n}(\mathbf{y}_i - \hat{y}_i)^2}{\sum_{i=1}^{n}(\mathbf{y}_i - \bar{y})^2}, \tag{10}$$

where n is the total number of input samples, y_i, $\hat{y}_i$, and $\bar{y}$ are the model-predicted SOH value, the real SOH value, and the average SOH value in each period, respectively. By encompassing these metrics, we can gain a deeper understanding of the model's performance in SOH estimation, identifying its strengths and weaknesses, which will serve as important guidelines for future model optimization.

4.2 Experimental results of CBAM-BiGRU

In the fields of machine learning and deep learning, the reasonable partitioning of training and testing data sets has a critical impact on the evaluation of model performance and the validation of its generalization capability. The training set aims to provide the essential learning basis and parameter optimization for the model, while the testing set is responsible for assessing the model's performance on unseen data, thereby ensuring its good generalization ability. Consequently, a scientifically sound partitioning strategy can effectively prevent overfitting and data leakage, while also maintaining consistency in data distribution between the training and testing sets.

In this study, we trained six individual battery cells (labeled as 25C02-25C03, 25C06-25C07, 35C02, and 45C02) under different temperature conditions (25, 35, 45 °C). At the same time, we tested four battery cells (labeled as 25C01, 25C05, 35C01, and 45C01) under different temperature conditions and with different battery cells to validate the model's capability to accurately predict the SOH of batteries under various temperature conditions. Notably, the focus of this study is on predicting the SOH of batteries in the range of 80%–100%, as a decline in SOH to 80% or below can significantly reduce the capacity and performance of the batteries and may adversely affect the charging and discharging efficiency.

Furthermore, we chose to make predictions while the battery is in an electrochemically stable state (i.e., in states I and V) when fully charged or fully discharged. This decision is based on the fact that the performance and impedance characteristics of the battery vary with the state of charge during the charging and discharging cycles. In states I and V, the battery is in a stable electrochemical state, where the internal chemical reactions and charge transfer processes are relatively consistent, thereby enhancing the model's prediction accuracy. Specifically, when the battery is fully charged or fully discharged, its chemical composition and conductivity stabilize, resulting in reduced polarization effects. This allows the EIS data to more accurately reflect the true state of the battery. Therefore, under these conditions, the model can learn the battery characteristics more effectively, improving prediction accuracy. Additionally, the rest period in state V helps mitigate polarization effects and promotes chemical equilibrium, allowing the battery's electrochemical reactions to reach a stable state, ultimately enhancing model performance.

4.2.1 SOH estimates under state I of SOC

In this section of the study, we conducted systematic experimental tests on different temperatures and various battery cells (including 25C01, 25C05, 35C01, and 45C01) under state I conditions, aiming to verify the effectiveness and accuracy of the proposed model in identifying the degradation mechanisms of battery SOH. As shown in Fig. 6, the relationship between the model predictions represented by the red curve and the actual measurements represented by the green curve is clearly displayed.

Through observation, it can be seen that the predicted curve has a very high degree of fit with the actual curve, showing significant overlap at several key points, which indicates that the model effectively captures and represents the subtle changes in the battery degradation process. This high level of consistency not only reflects the model's stability and sensitivity when handling complex EIS data but also validates its exceptional capability in data-driven feature extraction. Especially in the early stages of degradation, traditional models often struggle to accurately predict early changes due to the rapid decline. In contrast, the model proposed in this paper can timely capture the subtle changes in SOH, demonstrating superior predictive performance. As shown in Table 1, the error metrics for the 25C01 and 25C05 batteries are very close, indicating that our model successfully captures the complexity and degradation characteristics of different battery models during the charge and discharge cycles. Specifically, the RMSE for 25C01 is 0.0216, and the MAE is 0.0177, while the RMSE for 25C05 is 0.0272, with a MAE of 0.0213. These results suggest that under similar conditions, the

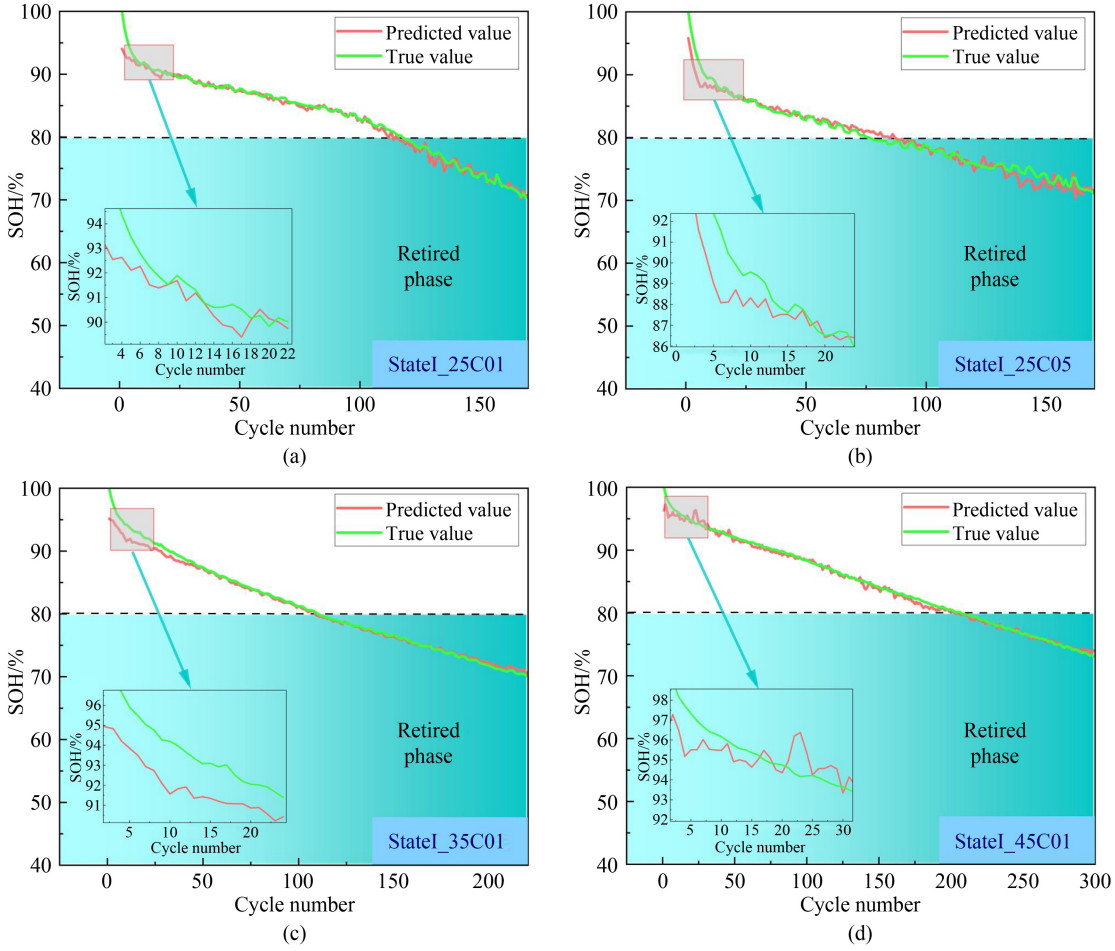

Fig. 6 SOH estimates result under State I of SOC: (a) 25C01; (b) 25C05; (c) 35C01; (d) 45C01.

Table 1 SOH estimation errors under SOC state I

Battery	Accuracy		
	RMSE	MAE	R^2
25C01	0.0216	0.0177	0.9272
25C05	0.0272	0.0213	0.9172
35C01	0.0187	0.0148	0.9606
45C01	0.0135	0.0099	0.9793

model exhibits good accuracy in predicting the SOH for both types of batteries.

We observed that although more training data can be obtained at 25 °C, the model performs better in predictions at 45 °C. This phenomenon can be attributed to the fact that as the temperature increases, the rate of internal chemical reactions within the battery accelerates, resulting in a significant enhancement of ionic conductivity in high-temperature environments and a decrease in the battery's EIS. Consequently, the range of variation in input features diminishes, and the similarity in the feature space between the training and testing data significantly increases. This enhanced similarity improves the machine learning model's ability to capture relevant features, allowing it to adapt to the data distribution more quickly and accurately, thus enhancing the precision of SOH predictions. For instance, at 45 °C, the model achieves an RMSE of 0.0135, with an R^2 value reaching 0.9793, further validating the model's superiority in high-temperature testing environments.

4.2.2 SOH estimates under state V of SOC

This subsection validates the capability of the proposed model to identify the SOH degradation mechanisms of the aforementioned batteries under SOC state V, with results presented in Fig. 7 and Table 2. In Figs. 7(a–d), the predicted curves for the four batteries show good consistency with the actual curves. Based on the comparison of Tables 1 and 2, the RMSE values for all batteries in the V state have significantly decreased, particularly for the 45C01, which shows a more pronounced improvement with its RMSE reduced from 0.0135 to 0.0110. This indicates a significant enhancement in the model's accuracy for predicting the health state of the battery in the V state. Similarly, the MAE in the V state has also shown remarkable improvement, especially with the MAE for the 45C01 dropping from 0.0099 to 0.0077, further validating the model's ability to capture subtle changes in the battery

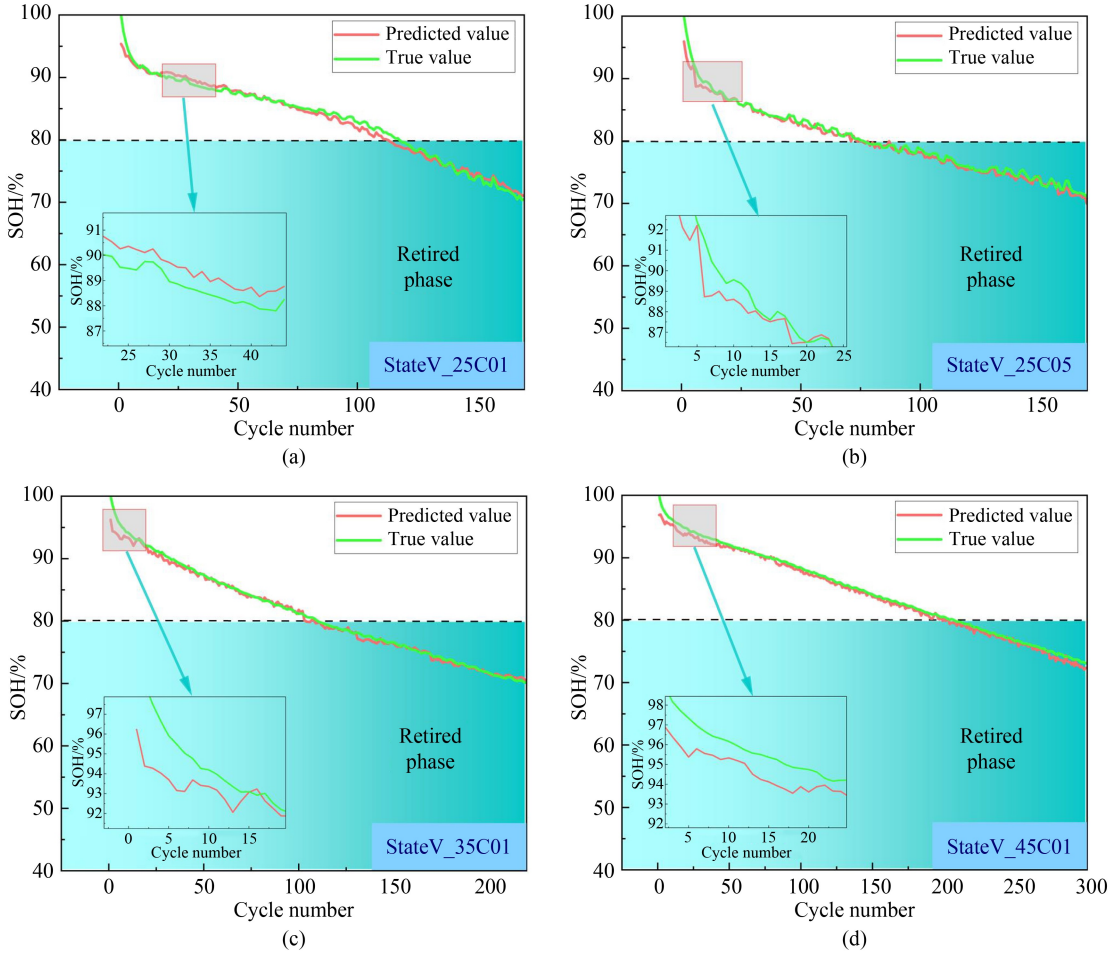

Fig. 7 SOH estimates result under State V of SOC: (a) 25C01; (b) 25C05; (c) 35C01; (d) 45C01.

Table 2 SOH estimation errors under SOC state V

Battery	Accuracy		
	RMSE	MAE	R^2
25C01	0.0194	0.0149	0.9376
25C05	0.0206	0.0187	0.9344
35C01	0.0168	0.0126	0.9675
45C01	0.0110	0.0077	0.9833

state more accurately under the current conditions.

This improvement can be attributed to the fact that in the I state, the battery is still in an active electrochemical reaction state prior to charging, resulting in higher internal resistance and a broader dynamic range. In contrast, in the V state, the battery enters a resting state after complete discharge, allowing the internal chemical reactions to reach a balance, which significantly enhances the stability of the feature data. This stability provides favorable conditions for the model to accurately capture changes in the battery state, thereby improving the precision of the predictions.

It is noteworthy that, although more training data can be obtained at 25 °C, the error metrics at different temperatures do not show significant differences; in some cases, the performance at 45 °C is even better. This is because, as the temperature rises, the reaction rates of the internal chemical processes in the battery increase, leading to a reduction in the EIS impedance of the battery. Consequently, the range of input feature variations narrows, which enhances the similarity between training and testing data. This facilitates the machine learning model's ability to capture relevant features, thereby improving prediction accuracy.

4.3 Comparison of estimation results with other models

In this study, we selected CNN-GRU, CBAM-GRU, and CBAM-BiGRU models for comparative experiments, aiming to comprehensively evaluate the performance of different architectures in predicting the SOH of batteries. By integrating these diverse model architectures, we can effectively compare various feature extraction and time series modeling approaches, thereby validating the superiority of the proposed models. To cover different operational scenarios as comprehensively as possible, this study chose to predict under different states (StateI_25C01, StateV_25C01), different temperatures (StateV_25C01, StateV_35C01, StateV_45C01), and different battery units at the same temperature

(StateV_25C01, StateV_25C05). This comprehensive experimental design, which considers various operational states, temperatures, and battery units, ensures the adaptability and robustness of the models.

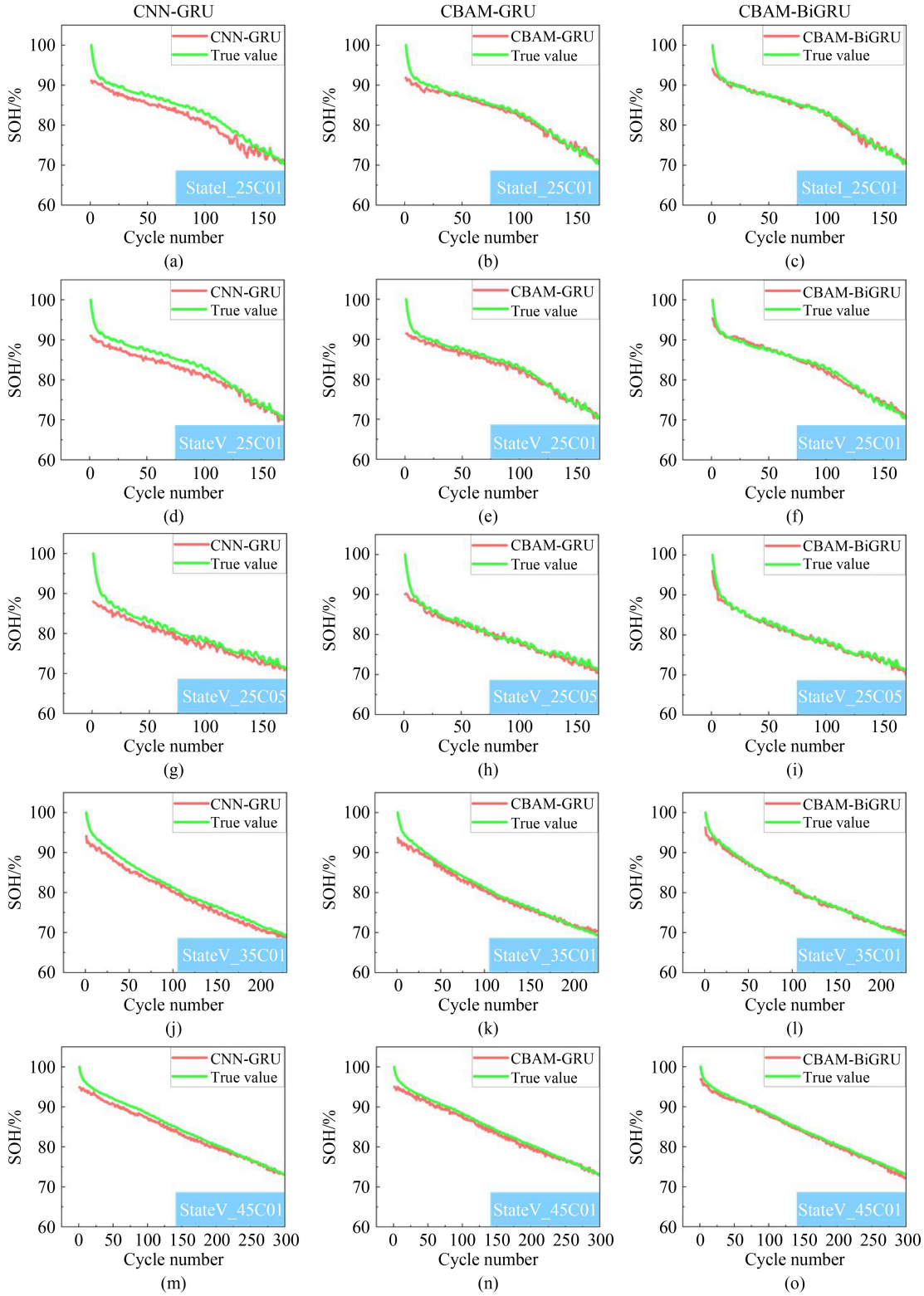

Fig. 8 Model comparison result: (a) CNN-GRU:StateI_25C01; (b) CBAM-GRU:StateI_25C01; (c) CBAM-BiGRU:StateI_25C01; (d) CNN-GRU:StateV_25C01; (e) CBAM-GRU:StateV_25C01; (f) CBAM-BiGRU:StateV_25C01; (g) CNN-GRU:StateV_25C05; (h) CBAM-GRU:StateV_25C05; (i) CBAM-BiGRU:StateV_25C05; (j) CNN-GRU:StateV_35C01; (k) CBAM-GRU:StateV_35C01; (l) CBAM-BiGRU:StateV_35C01; (m) CNN-GRU:StateV_45C01; (n) CBAM-GRU:StateV_45C01; (o) CBAM-BiGRU:StateV_45C01.

As shown in Fig. 8, the traditional CNN model struggles to extract key information from complex EIS image data. The prediction performance of CBAM-GRU surpasses that of CNN-GRU because CBAM-GRU can simultaneously integrate multiple information sources and utilize various feature representations, enhancing the model's complexity and expressive capability, which is particularly effective in handling the relationships within complex EIS image data. In contrast, the pure convolutional feature extraction method used by CNN-GRU may fall short when dealing with such tasks. Compared to both CNN-GRU and CBAM-GRU, the proposed CBAM-BiGRU demonstrates the best performance, primarily due to its ability to extract features from both past and future contextual information in the sequence. This bidirectionality allows the model to achieve a more comprehensive understanding of the input sequence.

The error results are shown in Table 3. Overall, the CBAM series models demonstrate significantly lower errors and higher interpretability compared to the traditional CNN-GRU model. Specifically, CBAM-BiGRU consistently exhibits the best performance across all states, indicating that the introduction of the attention mechanism and the bidirectional GRU structure significantly enhances the model's effectiveness in battery state prediction tasks. From the table, it can be observed that CBAM-BiGRU achieves the lowest RMSE across all states; particularly, in StateV_45C01, it reaches an RMSE of 0.0110, which shows a significant improvement in the model's accuracy for predicting battery states. Additionally, CBAM-BiGRU also significantly outperforms other models in terms of MAE, especially in StateV_45C01, where its MAE is 0.0077. This further confirms the reliability of the CBAM-BiGRU model in practical applications.

In summary, this study conducts a multidimensional error analysis across different states, temperatures, and battery cells, which not only validates the robustness of the model but also ensures the reliability of the experimental results. According to the error analysis results, the CBAM-BiGRU model excels in all performance metrics, further validating that the incorporation of the attention mechanism and BiGRU in deep learning models is an effective strategy for enhancing battery state prediction. This series of analyses illustrates the potential applications of deep learning models in battery state prediction, providing new perspectives and insights for future research and the development of battery management strategies.

Table 3 Model comparison result

Battery	Model	Accuracy		
		RMSE	MAE	R^2
StateI_25C01	CNN-GRU	0.0434	0.0313	0.8843
	CBAM-GRU	0.0284	0.0243	0.9121
	CBAM-BiGRU	0.0216	0.0177	0.9272
StateV_25C01	CNN-GRU	0.0398	0.0293	0.8947
	CBAM-GRU	0.0245	0.0175	0.9318
	CBAM-BiGRU	0.0194	0.0149	0.9376
StateV_25C05	CNN-GRU	0.0345	0.0267	0.9003
	CBAM-GRU	0.0263	0.0214	0.9234
	CBAM-BiGRU	0.0206	0.0187	0.9344
StateV_35C01	CNN-GRU	0.0278	0.0216	0.9267
	CBAM-GRU	0.0203	0.0183	0.9376
	CBAM-BiGRU	0.0168	0.0126	0.9675
StateV_45C01	CNN-GRU	0.0263	0.0198	0.9314
	CBAM-GRU	0.0176	0.0134	0.9614
	CBAM-BiGRU	0.0110	0.0077	0.9833

4.4 Comparison of model error results with different literature

This section validates the superiority of the proposed method by comparing it with the results from references [36] and [45]. Zhang et al. [45] introduced a simplified equivalent circuit model based on mid-to-low frequency EIS, which utilizes mid-to-low frequency EIS data sensitive to battery aging to estimate the SOH of lithium-ion batteries. In contrast, our method does not rely on the researchers' prior knowledge or feature engineering, thereby simplifying the manual feature extraction process while achieving prediction accuracy comparable to that reported in the literature.

Gou et al. [36] employed the convolutional and pooling layers of the VGG 16 neural network for unsupervised feature extraction from EIS images, integrating unsupervised feature extraction with SOH prediction within a neural network framework. In comparison, our study improves the feature extraction method for SOH; relative to the VGG 16 model, our approach requires fewer parameters and consumes less computational resources, while maintaining a predictive performance that is very close. Table 4 presents a comparative analysis of prediction errors between our method and other studies, demonstrating that the proposed method can accurately estimate the SOH of the battery. This further validates the effectiveness and superiority of our model.

5 Conclusions

In conclusion, this study presents an effective new

Table 4 Comparison results of the proposed method and similar studies

Literature	Battery	RMSE	MAE
This paper	StateI_25C05	0.0272	0.0213
	StateV_25C05	0.0206	0.0187
	StateI_45C01	0.0135	0.0099
	StateV_45C01	0.0110	0.0077
Ref. [45]	StateI_25C05	0.0190	0.0112
	StateV_25C05	0.0166	0.0113
Ref. [36]	StateI_45C01	0.0097	0.0083
	StateV_45C01	0.0048	0.0037

approach that integrates the CBAM with BiGRU for monitoring the health status of lithium-ion batteries through EIS. Initially, the raw EIS data are transformed into image data using the GAF. The application of CBAM then highlights key information features while minimizing irrelevant information, allowing for more accurate extraction of battery state parameters. The subsequent use of BiGRU for time series modeling captures the dynamic changes in SOH, thereby improving prediction accuracy under various environmental conditions.

Experimental results indicate that this method achieves a significant improvement in SOH estimation compared to traditional approaches, emphasizing the effectiveness of employing attention mechanisms in feature extraction and the robustness of BiGRU in temporal analysis. This research not only provides a viable deep learning solution for effective lithium-ion battery health management, but also demonstrates the potential of attention mechanisms in advancing battery state monitoring and assessment strategies.

Competing interests The authors declare that they have no competing interests.

References

1. Cui S, Lyu S, Ma Y, Wang K. Improved informer PV power short-term prediction model based on weather typing and AHA-VMD-MPE. Energy, 2024, 307: 132766
2. Kang L, Xu B, Li P, Wang K, Chen J, Du H, Liu Q, Zhang L, Lian X. Controllable preparation of low-cost coal Gangue-based SAPO-5 molecular sieve and its adsorption performance for heavy metal ions. Nanomaterials, 2025, 15(5): 366
3. Pan Y, Song J, Wang K. Research progress and prospects of liquid-liquid triboelectric nanogenerators: mechanisms, applications, and future challenges. ACS Applied Electronic Materials, 2024, 7(1): 1–12
4. Yang F, dos Santos E C, Jia X, Sato R, Kisu K, Hashimoto Y, Orimo S, Li H. A dynamic database of solid-state electrolyte (DDSE) picturing all-solid-state batteries. Nano Materials Science, 2024, 6(2): 256–262
5. Yang F, Wang Q, Cheng E J, Zhang D, Li H. User instructions for the dynamic database of solid-state electrolyte 2.0 (DDSE 2.0). Computers, Materials & Continua, 2024, 81(3): 3413–3419
6. Li P, Luo S, Zhang L, Liu Q, Wang Y, Lin Y, Xu C, Guo J, Cheali P, Xia X. Progress, challenges, and prospects of spent lithium-ion batteries recycling: a review. Journal of Energy Chemistry, 2024, 89: 144–171
7. Zhang H, Li Z, Liu Y, Du X, Gao Y, Xie W, Zheng X, Du H. Oxygen vacancies-modulated C-WO_3/BiOBr heterojunction for highly efficient benzene degradation. Vacuum, 2025, 234: 114117
8. Cao N, Du H, Lu J, Li Z, Lu J, Qiang Q, Lu H. Designing ionic liquid electrolytes for a rigid and Li+-conductive solid electrolyte interface in high performance lithium metal batteries. Chemical Physics Letters, 2025, 866: 141959
9. Liang L, Su M, Sun Z, Wang L, Hou L, Liu H, Zhang Q, Yuan C. High-entropy doping promising ultrahigh-Ni Co-free single-crystalline cathode toward commercializable high-energy lithium-ion batteries. Science Advances, 2024, 10(25): eado4472
10. Pan Y, Xu K, Wang R, Wang H, Chen G, Wang K. Lithium-ion battery condition monitoring: a frontier in acoustic sensing technology. Energies, 2025, 18(5): 1068
11. Pan Y, Xu K, Chen Z, Wang K. Advanced techniques for internal temperature monitoring in lithium-ion batteries: a review of recent developments. Coatings, 2025, 15(3): 268
12. Liang L, Li X, Su M, Wang L, Sun J, Liu Y, Hou L, Yuan C. Chemomechanically stable small single-crystal Mo-doped $LiNi_{0.6}Co_{0.2}Mn_{0.2}O_2$ cathodes for practical 4.5 V-class pouch-type Li-ion batteries. Angewandte Chemie International Edition, 2023, 62(11): e202216155
13. Pan Y, Wang G, Wang K. Frictional nanogenerators (TENGs) in medical health monitoring: a progress review. AIP Advances, 2025, 15(4): 040701
14. Wang K, Li L, Yin H, Zhang T, Wan W. Thermal modelling analysis of spiral wound supercapacitor under constant-current cycling. PLoS One, 2015, 10(10): e0138672
15. Liu W, Placke T, Chau K T. Overview of batteries and battery management for electric vehicles. Energy Reports, 2022, 8: 4058–4084
16. Shang Y, Wang S, Tang N, Fu Y, Wang K. Research progress in fault detection of battery systems: a review. Journal of Energy Storage, 2024, 98: 113079
17. See K, Wang G, Zhang Y, Wang Y, Meng L, Gu X, Zhang N, Lim K, Zhao L, Xie B. Critical review and functional safety of a battery management system for large-scale lithium-ion battery pack technologies. International Journal of Coal Science & Technology, 2022, 9(1): 36
18. Ren J, Ma J, Wang H, Yu T, Wang K. A comprehensive review on research methods for lithium-ion battery of state of health estimation and end of life prediction: methods, properties, and prospects. Protection and Control of Modern Power Systems, 2024
19. Yi Z, Wang S, Li Z, Wang L, Wang K. A novel approach for state of health estimation and remaining useful life prediction of supercapacitors using an improved honey badger algorithm assisted hybrid neural network. Protection and Control of Modern Power Systems, 2024, 9(6): 1–18
20. Wang S, Zhang J, Gharbi O, Vivier V, Gao M, Orazem M. Electrochemical impedance spectroscopy. Nature Reviews. Methods Primers, 2021, 1(1): 41
21. Li C, Yang L, Li Q, Zhang Q, Zhou Z, Meng Y, Zhao X, Wang L, Zhang S, Li Y, Lv F. SOH estimation method for lithium-ion batteries based on an improved equivalent circuit model via electrochemical impedance spectroscopy. Journal of Energy Storage, 2024, 86: 111167
22. Wu J, Meng J, Lin M, Wang W, Wu J, Stroe D. Lithium-ion battery state of health estimation using a hybrid model with electrochemical impedance spectroscopy. Reliability Engineering & System Safety, 2024, 252: 110450
23. Bao M, Liu D, Wu Y, Wang Z, Yang J, Lan L, Ru Q.

Interpretable machine learning prediction for Li-ion battery's state of health based on electrochemical impedance spectroscopy and temporal features. Electrochimica Acta, 2024, 494: 144449

24. Fleischer C, Waag W, Heyn H M, Sauer D U. On-line adaptive battery impedance parameter and state estimation considering physical principles in reduced order equivalent circuit battery models: Part 1. Requirements, critical review of methods and modeling. Journal of Power Sources, 2014, 260: 276–291
25. Xing Q, Zhang M, Fu Y, Wang K. Transfer learning to estimate lithium-ion battery state of health with electrochemical impedance spectroscopy. Journal of Energy Storage, 2025, 110: 115345
26. Tang T, Yuan H. The capacity prediction of Li-ion batteries based on a new feature extraction technique and an improved extreme learning machine algorithm. Journal of Power Sources, 2021, 514: 230572
27. Zhang H, Gao J, Kang L, Zhang Y, Wang L, Wang K. State of health estimation of lithium-ion batteries based on modified flower pollination algorithm-temporal convolutional network. Energy, 2023, 283: 128742
28. Qi G, Du G, Wang K. Progress in estimating the state of health using transfer learning-based electrochemical impedance spectroscopy of lithium-ion batteries. Ionics, 2025, 31(3): 1–13
29. Zhang Y, Tang Q, Zhang Y, Wang J, Stimming U, Lee A A. Identifying degradation patterns of lithium ion batteries from impedance spectroscopy using machine learning. Nature Communications, 2020, 11(1): 1706
30. Li Q, Li D, Zhao K, Wang L, Wang K. State of health estimation of lithium-ion battery based on improved ant lion optimization and support vector regression. Journal of Energy Storage, 2022, 50: 104215
31. Li Y, Zou C, Berecibar M, Nanini-Maury E, Chan J, Bossche P, Mierlo J, Omar N. Random forest regression for online capacity estimation of lithium-ion batteries. Applied Energy, 2018, 232: 197–210
32. Obregon J, Han Y R, Ho C W, Mouraliraman D, Lee C W, Jung J Y. Convolutional autoencoder-based SOH estimation of lithium-ion batteries using electrochemical impedance spectroscopy. Journal of Energy Storage, 2023, 60: 106680
33. Pradyumna T K, Cho K, Kim M, Choi W. Capacity estimation of lithium-ion batteries using convolutional neural network and impedance spectra. Journal of Power Electronics, 2022, 22(5): 850–858
34. Gou B, Xu Y, Feng X. State-of-health estimation and remaining-useful-life prediction for lithium-ion battery using a hybrid data-driven method. IEEE Transactions on Vehicular Technology, 2020, 69(10): 10854–10867
35. Li D, Yang D, Li L, Wang L, Wang K. Electrochemical impedance spectroscopy based on the state of health estimation for lithium-ion batteries. Energies, 2022, 15(18): 6665
36. Guo F, Huang G, Zhang W, Liu G, Li T, Ouyang N, Zhu S. State of Health estimation method for lithium batteries based on electrochemical impedance spectroscopy and pseudo-image feature extraction. Measurement, 2023, 220: 113412
37. Xing Q, Sun X, Fu Y, Wang K. Lithium-ion battery health estimate based on electrochemical impedance spectroscopy and CNN-BiLSTM-Attention. Ionics, 2025, 31(2): 1389–1403
38. Zhang C, Tu L, Zhou Z, Chen S, Wu J, Chen L. Estimating lithium-ion battery health using hybrid attention networks and multi-source data. IEEE Sensors Journal, 2024
39. Xu H, Li J, Yuan H, Liu Q, Fan S, Li T, Sun X. Human activity recognition based on Gramian angular field and deep convolutional neural network. IEEE Access:Practical Innovations, Open Solutions, 2020, 8: 199393–199405
40. Woo S, Park J, Lee J Y, Kweon I S. Cbam: convolutional block attention module. In: Proceedings of the European Conference on Computer Vision (ECCV), 2018: 3–19
41. Li Y, Dong B, Zerrin T, Jauregui E, Wang X, Hua X, Ravichandran D, Shang R, Xie J, Ozkan M, Ozkan C S. State-of-health prediction for lithium-ion batteries via electrochemical impedance spectroscopy and artificial neural networks. Energy Storage, 2020, 2(5): e186
42. Li P, Zhang Z, Xiong Q, Ding B, Hou J, Luo D, Rong Y, Li S. State-of-health estimation and remaining useful life prediction for the lithium-ion battery based on a variant long short term memory neural network. Journal of Power Sources, 2020, 459: 228069
43. Cui S, Joe I. A dynamic spatial-temporal attention-based GRU model with healthy features for state-of-health estimation of lithium-ion batteries. IEEE Access:Practical Innovations, Open Solutions, 2021, 9: 27374–27388
44. Sun R, Chen J, Li B, Piao C. State of health estimation for Lithium-ion batteries based on novel feature extraction and BiGRU-Attention model. Energy, 2025, 319: 134756
45. Zhang W, Li T, Wu W, Ouyang N, Huang G. Data-driven state of health estimation in retired battery based on low and medium-frequency electrochemical impedance spectroscopy. Measurement, 2023, 211: 112597